Polyhedron 197 (2021) 115046

Contents lists available at ScienceDirect

Polyhedron

journal homepage: www.elsevier.com/locate/poly

Selective and sensitive optical probe for the recognition of Zn (II) ion through turn-on optical response in aqueous medium: Experimental and theoretical approach

Mahantesh Budri [a], Ramesh Vadavi [a], Prajakta Kadolkar [b], Shivaraj Patil [b], Kalagouda Gudasi [a,*], Sanjeev Inamdar [b]

[a] Department of Chemistry, Karnatak University, Dharwad 580003, India
[b] Department of Physics, Karnatak University, Dharwad 580003, India

ARTICLE INFO

Article history:
Received 3 October 2020
Accepted 13 January 2021
Available online 23 January 2021

Keywords:
Optical sensor
Photostability
Reversible nature
TD-DFT study
Cytotoxicity
HeLa cells

ABSTRACT

A selective and sensitive Zn(II) ion responsive optical probe (*E*)-*N*′-(2, 4-dihydroxybenzylidene)-3, 5-di-*tert*-butyl-2-hydroxybenzohydrazide (**L**) was designed, synthesized and characterized. The optical behavior of **L** towards different metal ions were investigated using UV–Vis and Fluorescence techniques and results indicate its higher selectivity for Zn(II) ion. The experimental results of **L** for Zn (II) are correlated with computational results. The probe exhibits weak fluorescence due to *cis–trans* isomerization and exited state intra molecular proton transfer (ESIPT) behavior in 4% aqueous acetonitrile solution. However, in the presence of Zinc (II) ion, —C═N— isomerization and ESIPT processes are inhibited due to its coordination to metal ion by triggering CHEF (chelation-enhanced fluorescence) giving turn-on fluorescence response. The Job's plot and B-H (Banesi- Hildebrand) experimental results indicate 1:1 stoichiometry between host-guest interaction. The association constant of **L** for Zn^{2+} ion was found to be 3.9×10^{7} M^{-1} with nanomolar level of detection. The pH studies indicate that, the probe could work at physiological conditions. The reversible, highly photostable optical probe could recognizes the presence of Zn^{2+} ion in HeLa cells.

1. Introduction

Because of its applications in various fields of science such as chemistry, biology, medicine, environment *etc*., molecular recognition remains to be a most preferred area for researchers and it is one of the cornerstones of supramolecular chemistry [1]. The information obtained at supramolecular level, when molecules interact with substrate is represented by molecular recognition events which causes a change in the physical and chemical properties of molecules and so translate themselves into generation of useful signals. Its usage in the selective recognition of biologically, environmentally, medicinally and industrially important metal ion/s is attracting much attention [2].

Nowadays, the most intense research area in chemical biology and supramolecular chemistry is the development of new molecules for sensing different kind of cations, anions and to some extent neutral molecules also [3,4]. Design and synthesis of new chemical compounds for sensing cations especially "3d group" elements remains to be an interesting area in research because of their irreplaceable biological, industrial and environmental applications [5–7]. Zinc is the second most abundant heavy metal ion in human body next to iron. Presence of normal concentration of Zinc plays crucial role in many physiological and biochemical processes [8] but its abnormality induces many serious problems on human health as well as environmental processes [9].

The basic principle involved in the molecular sensing is the Pearson's HSAB concept. According to this concept, Zn^{2+} ion is considered as the borderline Lewis acid. Hence, by selecting borderline Lewis bases (aniline, pyridine, N^{3-}, Br^{-}, NO^{2-}, SO_3^{2-}, N_2) as binding groups, the Zinc ion selectivity of the molecular probe over other interfering hard (Na^{+}, K^{+}, Mg^{2+}, Ca^{2+}, Mn^{2+}, Cr^{3+} and Fe^{3+}), soft (Cu^{+}, Ag^{+}, Hg^{2+} and Cd^{2+}) Lewis acids and some of bio-relevant borderline Lewis acids (Fe^{2+}, Co^{2+}, Ni^{2+} and Cu^{2+}) could be achieved [10,11]. Zinc with completely filled "3d" shell is spectroscopically and magnetically silent. Upon interaction with probe, Zinc modulates many photophysical properties of probe through many signalizing processes in the excited state [12,13].

An analytical techniques reported in the literature for the recognition of Zinc suffers with one or other disadvantages. Therefore,

* Corresponding author.
E-mail address: drkbgudasi@kud.ac.in (K. Gudasi).

https://doi.org/10.1016/j.poly.2021.115046
0277-5387/

Table 1
Comparison of recently reported Zinc sensor with present study.

Sl. No	Probe structure	Ka/log Ka	LOD	Solvent	Mode of sensing	Application	Ref.
1	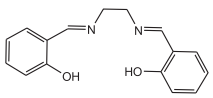	———	20×10^{-6} M	aq. methanol	Inhibiting PET process	Logic gate	[20]
2.	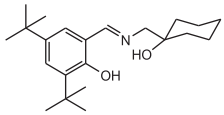	5×10^{4} M^{-1}	7.2×10^{-7} M	aq. methanol	Inhibiting PET process	Cell imaging	[21]
3.	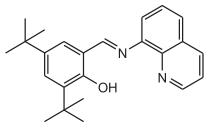	————	1.5×10^{-8} M	aq. ethanol	Inhibiting PET and -C=N isomerization process	Cell imaging	[22]
4.	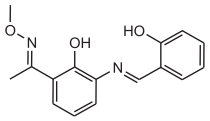	2.2×10^{4} M^{-1}	1.4×10^{-7} M	aq. methanol	Inhibiting PET process & activating CHEF process	————	[23]
5.	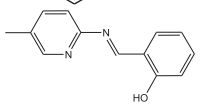	5.6×10^{4} M^{-1}	1.13×10^{-7} M	DMSO	ICT Process	———	[24]
6.	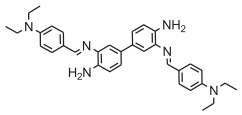	7.8×10^{4} M^{-1}	8.6×10^{-9} M	DMF	Inhibiting -C=N isomerization process and CHEF process	————	[25]
7.	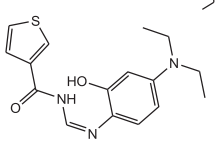	2.1×10^{4} M^{-1}	3×10^{-8} M	DMSO:H_2O	Activation of CHEF	Cell imaging	[26]
8.	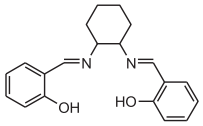	3.7×10^{4} M^{-1}	———	Ethanol	Inhibiting -C=N isomerization process and CHEF process	——	[27]
9.	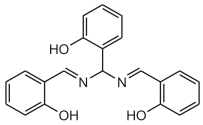	16.2×10^{3} M^{-1}	5×10^{-8} M	Methanol	Inhibiting PET process & activating CHEF process	Logic gates	[28]
10.	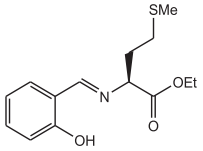	5.3×10^{3} M^{-1}	5×10^{-7} M	HEPES buffer solution of pH 7.2 prepared in CH_3CN/H_2O	Inhibiting PET process & activating CHEF process	Bio-imaging	[29]
11.	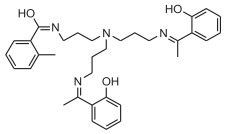	3×10^{6} M^{-1}	8.8×10^{-8} M	Tris-HCl buffer	Inhibiting PET process & activating CHEF process	Water sample analysis	[30]
12.	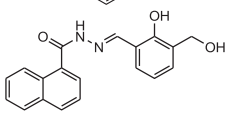	1.1×10^{5} M^{-1}	3.1×10^{-9} M	THF: H_2O in HEPES buffer	Inhibition of ESIPT and —C=N isomerization	Cell imaging	[31]
13.	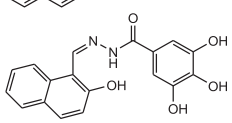	1.6×10^{5} M^{-1}	9.3×10^{-8} M	DMSO:H_2O	CHEF	Test strips	[32]
14.	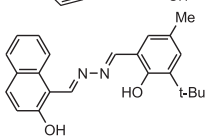	4.6×10^{4} M^{-2}	1.3×10^{-8} M	100% aqueous solution	Inhibition of PET CHEF Process	Water and food sample analysis	[33]
15.		1.5×10^{5}	1.1×10^{-7}	DMF:H_2O	CHEF and AIEE process	Paper strips	[34]

Table 1 (*continued*)

Sl. No	Probe structure	Ka/log Ka	LOD	Solvent	Mode of sensing	Application	Ref.
	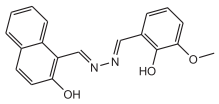	M^{-1}	M				
16.	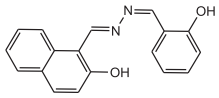	1.8×10^5 M^{-1}	46×10^{-9} M	DMF:H_2O	AIE	Biological and environmental samples	[35]
17.	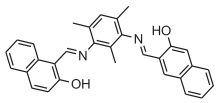	1.1×10^5 M^{-1}	1.47×10^{-7} M	ACN:H_2O	Inhibition of ESIPT and —C═N isomerization	cell imaging	[36]
18.	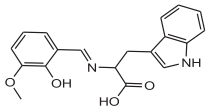	3.6×10^5 M^{-1}	1.1×10^{-8} M	Double Distilled water	Fluorescence enhancement inhibition of —C═N isomerization	Cell imaging	[37]
19.	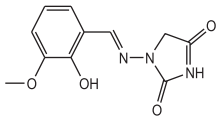	4.5×10^3 M^{-1}	12×10^{-6} M	bis-tris buffer	Fluorescence enhancement CHEF	Cell imaging	[38]
20.	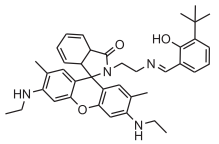	4.8×10^4 M^{-1}	77×10^{-9}M	CH_3OH:H_2O	Fluorescence enhancement inhibition of PET and CHEF	Cell imaging	[39]
21.	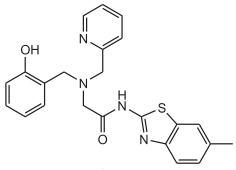	4.10	205 nM	Ethanol	CHEF	————	[40]
22.	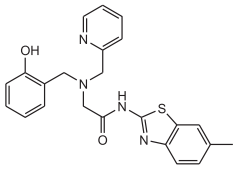	4.91	357 nM	EtOH:H_2O	CHEF	——	[41]
23.	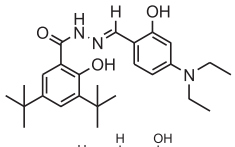	9.6×10^6 M^{-1}	8×10^{-9} M	ACN	Blocking of ESIPT and -C═N isomerization and activation of CHEF process	Cell imaging	[42]
24.	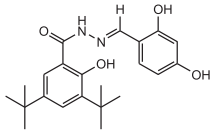	3.9×10^7 M^{-1}	14×10^{-9} M	ACN: H_2O	Blocking of ESIPT and -C═N isomerization and activation of CHEF process	Cell imaging	This work

there is a need of newer methods with enhanced accuracy and precision [14]. Recent literature suggests that, use of UV–Vis and fluorescence technique for monitoring transition metal ions using chemosensor is strongly valid because of their higher selectivity, sensitivity, fast response, simple handling and large Stokes shift [15].

Fluorescent chemesensors are the molecules of abiotic origin, which upon interaction with target analyte/s give fluorescence signal [16,17]. On interacting with the analyte, the fluorescence intensity of the probe either, i) increases called as turn on fluorescence ii) decreases called as a turn off fluorescence (quenching), or iii) there will be a shift in the fluorescence signal. Because of their simplicity, easy mode of detection, forefront applications, turn-on optical sensors dominate over other category [18].

Hydrazone derivatives are the powerful tool for sensing different cations due to their facile synthesis, low-cost, simplicity, sensitivity and structural framework [6] and the resulting Zinc complexes are well known for their electronic, photophysical and biological applications [7]. In literature, many chemosensors based on coumarin, anthracenone, quinolone, benzazole, BINOL, fluorescein, and rhodamine fluorophores have been reported to recognize Zinc ion [19] but *tert*-butyl group substituted aromatic systems are

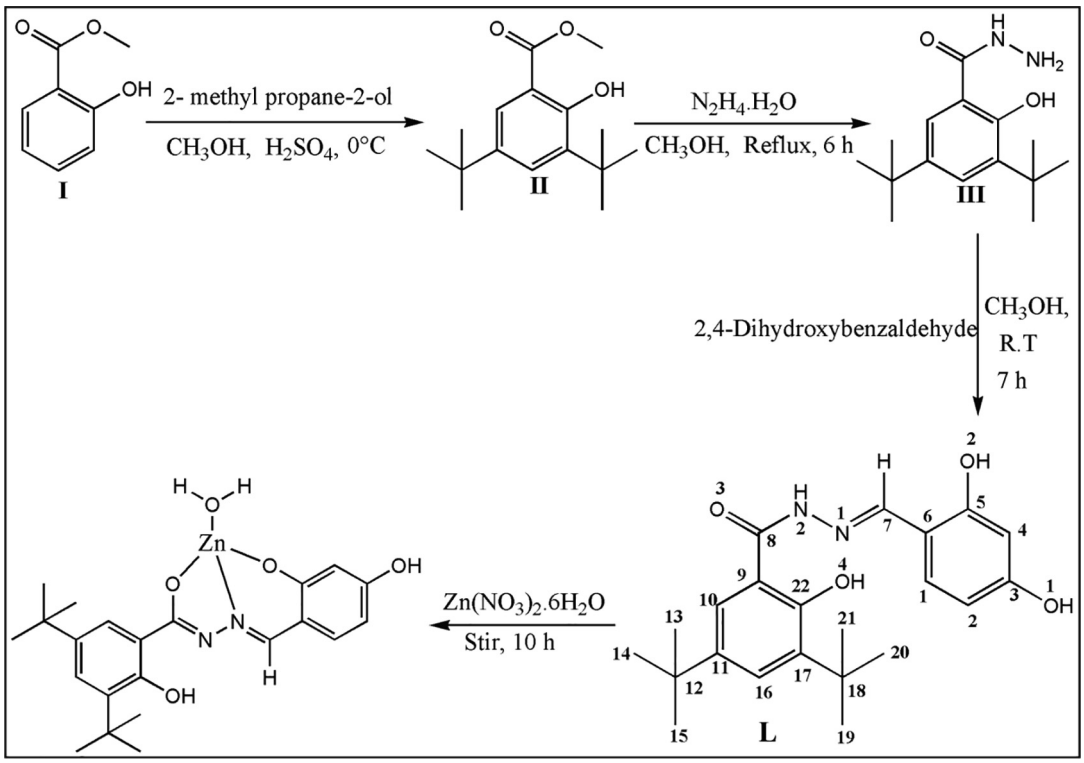

Scheme 1. Synthesis of L and its coordinating mode towards Zinc ion.

Fig. 1a. Color change of L (1×10^{-5} M soln. in 4% aq. CH_3CN) upon addition of Zinc ion (1×10^{-3} M soln. in 4% aq. CH_3CN).

less explored. These groups are well known to increase the solubility in organic solvents. Synthesizing hydrazone derivatives of desired fluorescence property by incorporating fluorescence assisting groups in their structure is the attractive weapon for sensing metal ions with higher accuracy and precision. Any molecule to be an efficient sensor for Zinc ion based on specific excitation processes (ESIPT/ICT), then it should exhibit some important photophysical characteristics as given below.

a) The molecule should exhibit ICT character and upon coordination with metal it should increase.
b) The presence of azomethine group enhances the fluorescence intensity of probe upon coordination with Zinc ion.
c) Presence of acidic and basic moieties within sensor initiates ESIPT process and it can be deactivated upon coordination with Zinc to enhance its fluorescence intensity.

The photophysical properties of 3,5-di-*tert*-butyl-2-hydroxybenzohydrazone obtained by condensing 3,5-di-*tert*-butyl-2-hydroxybenzohydrazide with 2,4 dihydroxybenzaldehyde are very close to the above expectations. Therefore, in continuation with our earlier work, in the present study we have synthesized a novel optical sensor (*E*)-*N*'-(2, 4-dihydroxybenzylidene)-3, 5-di-*tert*-butyl-2-hydroxybenzohydrazide (**L**). It selectively senses Zn(II) ion over other interfering metal ions in 4% aqueous acetonitrile medium with nanomolar level of detection limit. Table 1 depicts the comparison of some of the aspects of recently reported Zinc sensors with the present sensor. The reported sensor exhibits higher binding constant with lower detection limit.

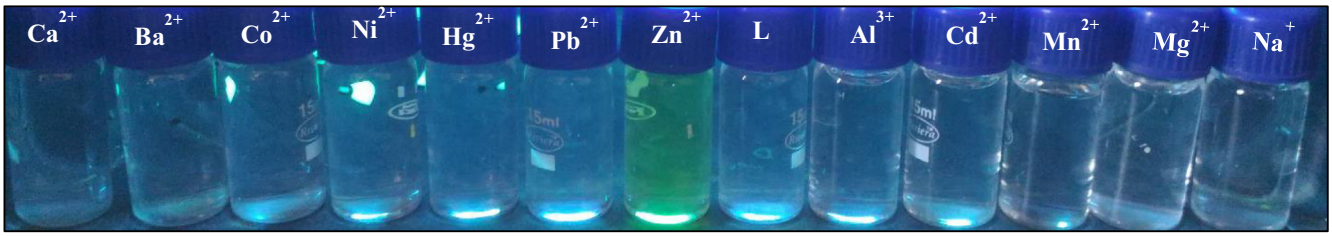

Fig. 1b. Color change of L (1×10^{-5} M soln. in 4% aq. CH_3CN) after the addition of an equiv. of respective cations (1×10^{-3} M soln.) in 4% aq. CH_3CN.

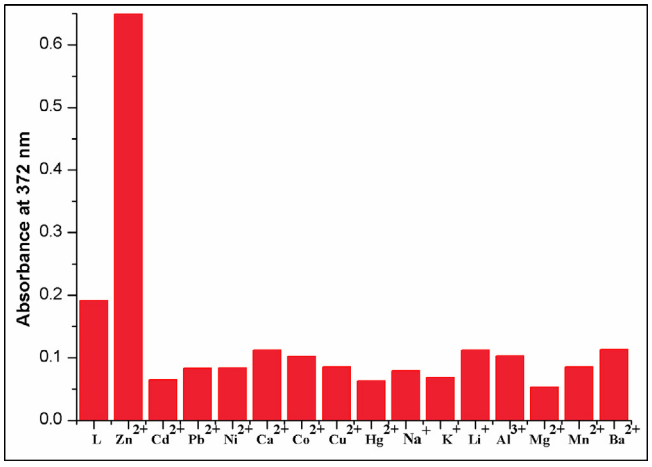

Fig. 2. Relative absorbance of probe at 372 nm upon interaction with various metal ions.

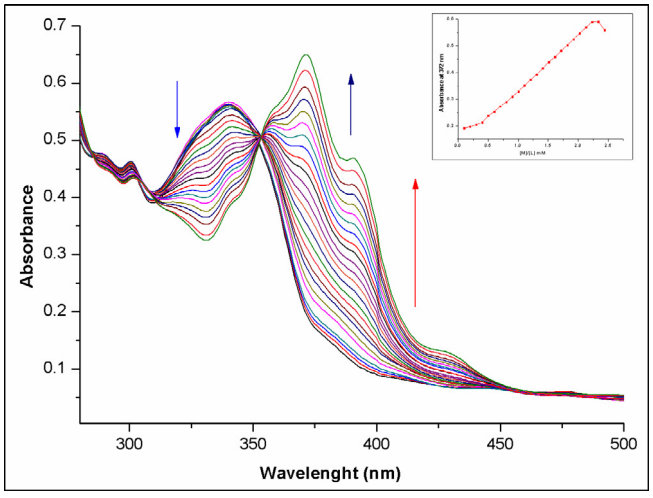

Fig. 3. Electronic spectral changes of L (1×10^{-5} M) in the presence of different concentrations of Zn^{2+} ions in 4% aq. CH_3CN. Inset: UV–Vis absorbance at 372 nm versus the number of equiv. of Zn^{2+} added.

2. Experimental section

2.1. Synthesis of optical probe

Synthetic path for fluorophore is shown in Scheme 1.

3, 5-di-*tert*-butyl-2-hydroxybenzohydrazide was prepared by the reported method [42]. Methanolic solution of 2, 4-dihydroxybenzaldehyde (2 g, 14.5 mmol) was slowly added to a methanolic solution of 3, 5-di-*tert*-butyl-2-hydroxybenzohydrazide (3.8 g, 14.5 mmol) and stirred for 7 h at room temperature. Completion of the reaction was monitored by TLC. The precipitate obtained was filtered, washed with cold methanol and dried in air.

Color: Light yellow: 89%, m.p: 265 °C, Anal. Calcd for $C_{22}H_{28}N_2O_4$ (%): C, 68.73.; H, 7.34; N, 7.29. Found (%): C, 68.69; H, 7.30; N, 7.32. IR (cm^{-1}): 3470 (O—H), 3187 (N—H), 1631 (C=O), 1616 (C=N). ^1H NMR (400 MHz, DMSO d_6, ppm): 1.30 (9H, s, *tert*-Bu, C13H, C14H, C15H), 1.37 (9H, s, *tert*-Bu, C19H, C20H, C21H), 7.71 (1H, d, C1H, J = 2 Hz), 6.33 (1H, d, C4H, J = 2.4 Hz), 7.43 (1H, d, C16H, J = 2 Hz), 11.99 (1H, s, N2H), 13.08 (1H, s, O4H), 12.25 (1H, s, O2H), 10.00 (1H, s, O1H), 7.42 (1H, d, C10H, J = 2 Hz), 8.64 (1H, s, C7H), 6.33 (1H, d, C4H, J = 2.4 Hz); ^{13}C NMR (100 MHz, DMSO d_6, ppm): 31.30 ($(CH_3)_3$), 34.22 ($(CH_3)_3$), 29.21 (C-$(CH_3)_3$), 34.71 (C-$(CH_3)_3$), 112.18 (C6), 158.32 (C7), 167.01 (C8), 136.54 (C17), 128.24 (C16), 139.69 (C11), 121.15 (C10), 110–140 (C1-C4, aromatic). EI-MS: m/z – 384 $[M]^+$.

2.2. Synthesis of zinc complex

A 4% aqueous acetonitrile solution of $Zn(NO_3)_2{\cdot}6H_2O$ (0.77 g, 2.6 mmol) was slowly added to the 4% aqueous acetonitrile solution of **L** (1 g, 2.6 mmol) with constant stirring for 10 h. The yellow solid obtained was filtered, washed with cold 4% aqueous acetonitrile and dried in air.

Color: Yellow, yield: 75%, m.p: 340 °C, Anal. Calcd. for $C_{22}H_{28}N_2O_5Zn$ (%): C, 56.72; H, 6.06; N, 6.01; Zn 14.04. Found (%): C, 56.80; H, 6.14; N, 6.05; Zn 12.40. IR (cm^{-1}): 3489 (O—H), 1575(C=N), 1617 (C=N, new), 1128 (C—O). ^1H NMR (400 MHz, DMSO d_6, ppm): 1.29 (9H, s, *tert*-Bu, C14H, C15H, C16H), 1.39 (9H, s, *tert*-Bu, C20H, C21H, C22H), 8.54 (1H, s, C7H), 14.13 (1H, s, O4-H), 6.00–8.00 (Ar-H), ESI-MS (m/z): 467 $[M + H]^+$. Molar conductance ($\Omega^{-1}cm^2$ mol^{-1}): 3.35.

2.3. Cytotoxicity assay and bioimaging experiment

The cytotoxic effect of probe and its Zinc complex on HeLa cells was ascertained by MTT assay. HeLa cells were grown in tissue culture flask in Dulbecco's modified Eagle medium (DMEM) supplemented with 10% (v/v) fetal bovine serum (FBS) + penicillin (100 g/mL) + streptomycin (100 μg/mL) at 37 °C in a CO_2 incubator. HeLa cells were plated (approximately 10^4 cells per well) into a 96-well flat-bottom micro plate and grown at 37 °C in 95% humidity and 5% CO_2 for overnight. After that, HeLa cells were incubated with different concentrations of **L** and its Zinc complex in DMEM solution for period 24 h. The cells were washed with phosphate buffer solution and 20 μL of the MTT staining solution was added to each well and incubated at 37 °C for 5 h. 100 μL of dimethyl sulfoxide was added to each well to dissolve formazan crystals formed and absorbance was recorded at 570 nm using micro plate reader (ELISA) [43].

For cell imaging experiment, cultured HeLa cells were treated with the 10 μM of probe and incubated separately for 30 min at 37 °C in dark. HeLa cells were washed with PBS buffer and corresponding images were taken. Later on, 10 μM of Zinc was incubated for 4 h and respective photographs were captured [44].

3. Results and discussion

3.1. UV–Vis absorption titration of Zinc (II) ion

The electronic spectrum of probe (1×10^{-5} M) in 4% aqueous acetonitrile exhibits three absorption maxima at 340, 299 and 290 nm. The electronic properties of **L** with various metal ions (*viz.*; Al^{3+} ($M(NO_3)_3$)), Ca^{2+}, Ba^{2+}, Mg^{2+}, Mn^{2+}, Ni^{2+}, Zn^{2+}, Cu^{2+}, Co^{2+}, Cd^{2+}, Pb^{2+}, Hg^{2+} ($M(NO_3)_2$) and K^+, Li^+, Na^+ ($M(NO_3)$ was pursued in 4% aqueous acetonitrile. Amongst various metal ions (10 equivalent of each) tested, only Zn^{2+} ion induces significant change in the electronic spectrum of **L** showing its higher selectivity for Zn^{2+} ion (Fig. S9). Colorless solution immediately turns to intense yellow (Figs. 1–2). Upon the addition of Zn^{2+} ion, the intensity of bands at 340, 299 and 290 nm have decreased and at the same time three new bands at 429, 390 and 372 nm have appeared. The formation of equilibrium points at 310 and 353 nm confirms the transformation of free **L** into its Zinc complex (Fig. 3) [44].

Upon slowly titrating Zinc ion with **L**, intensity of bands at 429, 390 and 372 nm increases while that of 340, 299 and 290 nm decreases till saturation point is reached. A band at 340 nm exhibits 15 nm blue shift due to increased ICT character of L due to for-

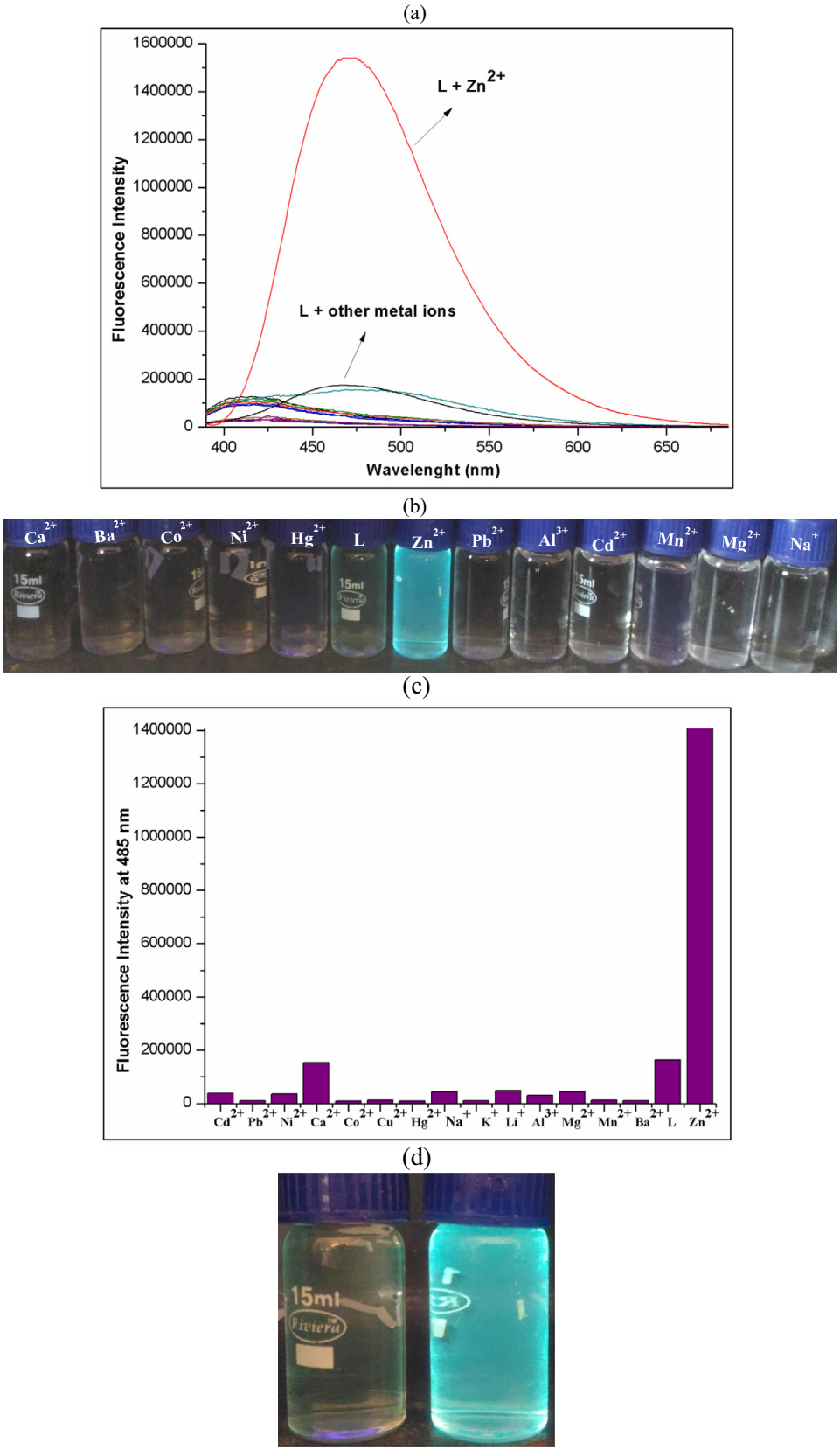

Fig. 4. Electronic spectral changes of L ($1x10^{-5}$ M) in the presence of different concentrations of Zn^{2+} ions in 4% aq. CH_3CN. Inset: UV–Vis absorbance at 372 nm versus the number of equiv. of Zn^{2+} added.

mation of Zinc complex (which increases the planarity of probe) with extended conjugation by exhibiting greater electron delocalization [45]. The data obtained from absorption titration profile

were fitted to the Benesi-Hildebrand equation to get the dissociation constant.

$$\frac{Amax - A0}{A - A0} = 1 + \frac{1}{Kd}[M]^n$$

where, A_0 and A_{max} are the absorbance of the ligand in the absence and presence of the metal ion respectively. Binding constant was determined from the slope of the linear plot and it is found be 1.11×10^7 M^{-1} (Fig. S11) [24,46,47]. The limit of detection reaches to 1.85×10^{-7} M (Fig. S10) [48].

3.2. Fluorescence titration of Zinc (II) ion

When excited at 340 nm, probe shows weak emissive band at 481 nm (Φ = 2.5%). The various metal ions (*viz.*; Al^{3+} ($M(NO_3)_3$)), Ca^{2+}, Ba^{2+}, Mg^{2+}, Mn^{2+}, Ni^{2+}, Zn^{2+}, Cu^{2+}, Co^{2+}, Cd^{2+}, Pb^{2+}, Hg^{2+} ($M(NO_3)_2$) and K^+, Li^+, Na^+ ($M(NO_3)$ were added to the solution of probe to check its emissive response. We noticed that, only Zinc (II) ion induces remarkable changes in the emission spectrum of probe, indicating its higher selectivity for Zinc ion (Fig. 4). Upon addition of Zinc ion, probe shows a 10-fold higher fluorescence intensity with small red shift of emission maxima (Φ = 2.8%) [13,49–51].

The concentration dependent profile shows that, by incremental addition of Zinc (II) ion, the fluorescence intensity of fluorophore goes on increasing till 1:1 stoichiometry is reached (Fig. 5). The detection limit of probe for Zinc (II) ion was found to be 14 nM using the IUPAC approved equation $3\sigma/S$ (where σ is the standard deviation of ten blank samples and S is the slope of the calibration curve) (Fig. 6) [52]. The association constant was calculated using emission titration data and it is found to be 3.9×10^7 M^{-1} (Fig. 7) [47].

3.3. Plausible mechanism for turn-on fluorescence sensing

The weak fluorescence intensity of the bare probe upon excitation at 340 nm is due to (i) free rotation around the imine bond and (ii) occurrence of ESIPT process. As shown in Supplementary data (Figs. S19 & S20), the expanded form of ^{1}H NMR spectrum of probe shows small humps (of low intensity) in addition to major peaks due to cis-trans isomerization. We have also tried to resolve these peaks by recording spectrum at lower temperature but failed due to its solubility problem in $CDCl_3$. The free rotation around the imine bond of **L** got restricted when Zinc ion binds with it which leads to the formation of a rigid structure by activating the chelation enhanced fluorescence (CHEF) process [24,53,54]. On the other side, the strength of hydrogen bond is greatly affected by solvents as well as metal ions where the cleavage of intramolecular hydrogen bonds quenches the ESIPT fluorescence in highly polar solvents such as alcohol, dimethylformamide (DMF) and DMSO. The transfer of electrons from the imine nitrogen to the aromatic system leads to the quenching of intensity. However, coordination of the imine nitrogen to Zn^{2+} ion leads to suppressing of ESIPT process. ESIPT process in **L** may be inhibited upon the addition of Zinc ion which causes deprotonation of hydroxyl groups responsible for ESIPT process. The deprotonation leads to increased ICT character in **L** due to increment in its planarity by extended conjugation leading to a high fluorescence (Scheme 2). An occurrence of ESIPT process and greater involvement of the ICT character of receptor in the excited state of complex was well supported by large Stokes shift (141 nm) [13,24,55–57].

3.4. Binding mode and stoichiometry studies

To know the coordinating mode of **L** for Zinc ion, different techniques were adopted. ^{1}H NMR spectrum of free **L** in DMSO d_6 con-

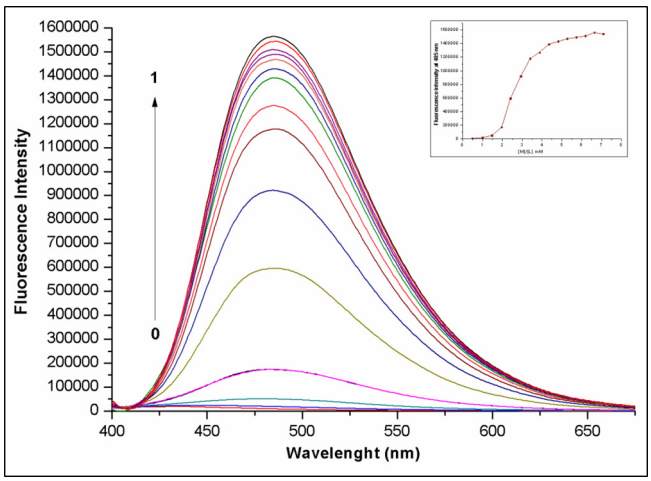

Fig. 5. Fluorescence spectral changes of probe ($1x10^{-5}$ M) in the presence of different concentrations of Zinc (II) ion with an excitation at 340 nm in 4% aq. CH_3CN. Inset: Fluorescence intensity at 485 nm versus the number of equivalents of Zn^{2+} added.

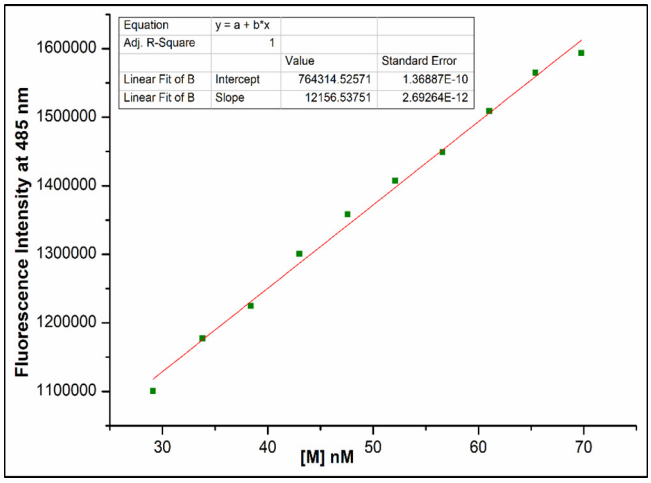

Fig. 6. Limit of detection based on change in the ratio (fluorescence intensity at 485 nm) of L with Zn^{2+}.

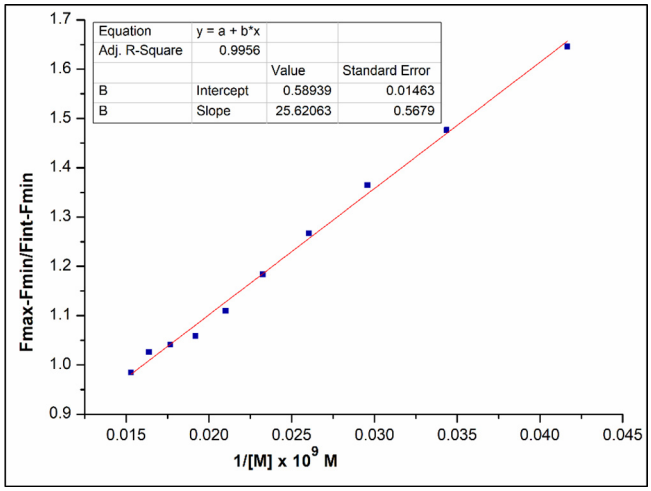

Fig. 7. Benesi-Hildebrand plot (fluorescence intensity at 485 nm) for L (1×10^{-5} M) based on fluorescence titration, assuming 1:1 ratio for association between L and Zn^{2+}.

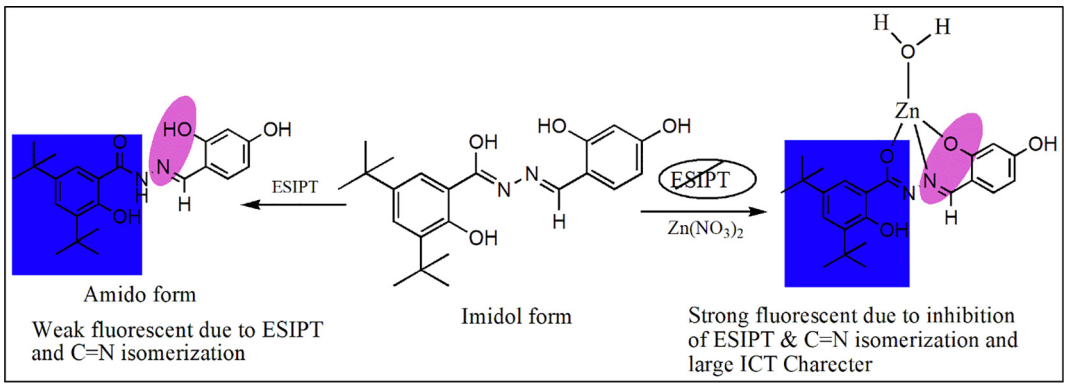

Scheme 2. The proposed sensing mechanism between L and Zn^{2+}.

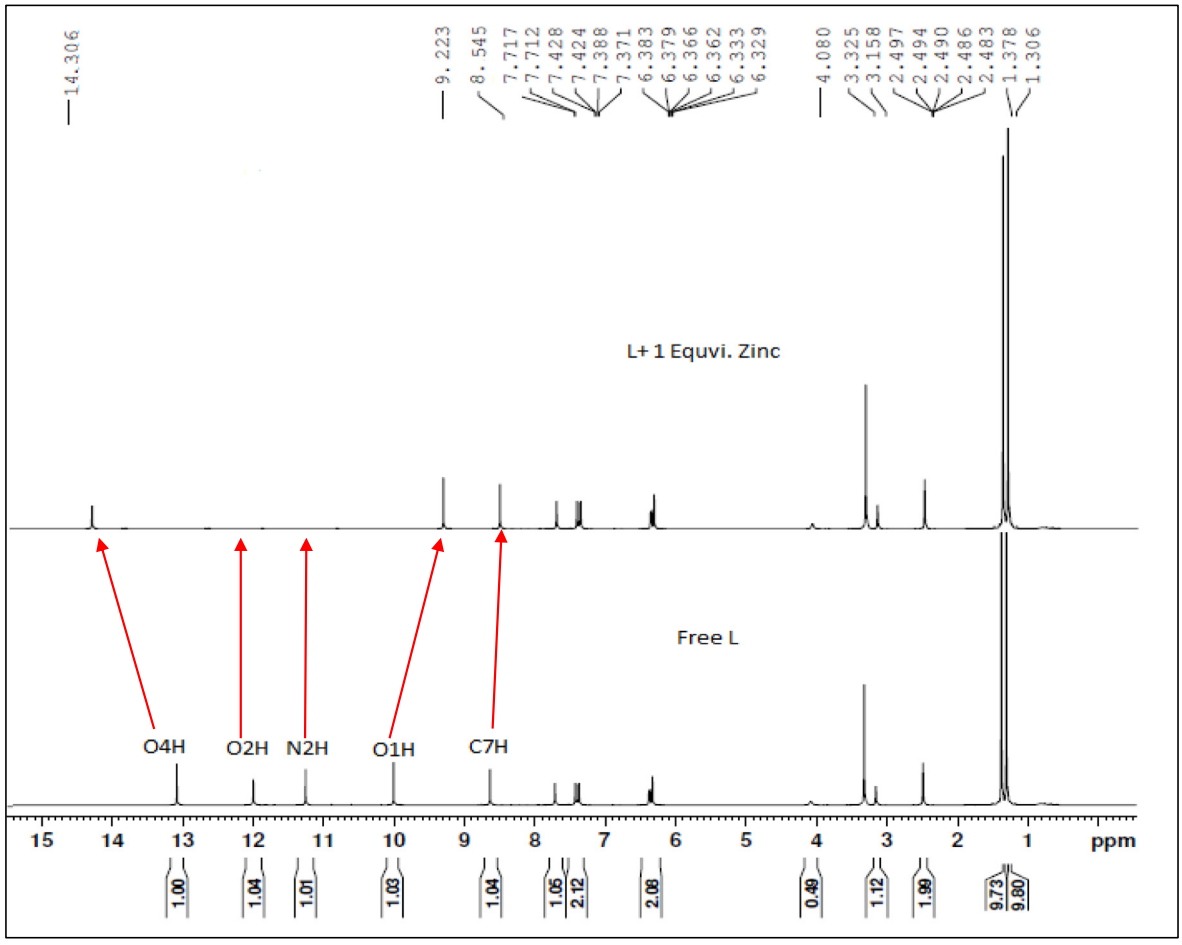

Fig. 8. Job's plot for the binding of L with Zn^{2+} in 4% aq. CH_3CN (Fluorescence intensity at 485 nm was plotted as a function of the molar ratio $[Zn^{2+}]/([L] + [Zn^{2+}])$).

tains signals at 13.08, 11.99, 11.25, 10.00 and 6.63 ppm assigned to O4H, O2H, N2H, O1H and C7H protons respectively and remaining protons resonate in their expected region. The protons of O2H and N2H vanishes completely upon adding an equivalent of Zinc ion due to their strong involvement in coordination. A peak at 13.08 ppm has shifted to 14.30 ppm due to participation of O4H proton in hydrogen bonding during complexation. The peaks at 10.00 and 6.63 ppm of O1H and C7H protons have shifted to 9.22 and 8.56 ppm respectively due to change in electron density around these protons (Fig. 8). The ^1H NMR titration experiment suggest the interaction of **L** to Zn^{2+} through its *ONO* donor set of atoms *via* deprotonation of O2H and N2H protons through *keto-enol* tautomerism (Scheme 1).

The positive mode ESI-MS spectrum of probe shows a molecular ion peak at *m/z*: 385 which corresponds to [L-H] $^+$. A new peak appeared at *m/z*: 467 upon the addition of an equivalent of Zinc ion corresponds to $[\mathbf{L} + Zn^{2+} + H_2O + H]^+$ indicating 1:1 stoichiometry between host–guest interaction (Fig S7). Job's experimental results further support 1:1 stoichiometry between probe and Zinc, where the maximum fluorescence intensity/absorbance was achieved near 0.5 mol fraction (Fig. 9 & S12) [45].

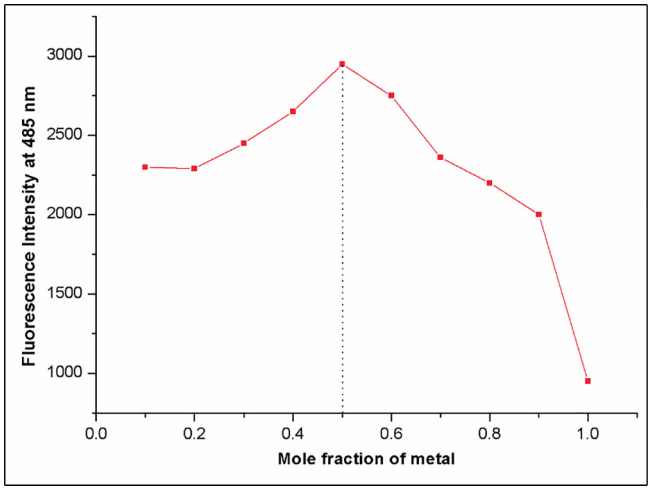

Fig. 9. Job's plot for the binding of L with Zn^{2+} in 4% aq. CH_3CN (Fluorescence intensity at 485 nm was plotted as a function of the molar ratio $[Zn^{2+}]/([L] + [Zn^{2+}])$).

3.5. Geometry optimization and electronic structure

To correlate experimental results with theoretical results and explore the sensing mechanism between host–guest interaction, computational studies were performed. The energy minimized structures of **L** and **L**-Zn^{2+} are shown in Fig. 10. The information of electronic properties of **L** and **L**-Zn^{2+} was obtained by analyzing the HOMO (Highest occupied molecular orbital) and the LUMO (Lowest unoccupied molecular orbital) (Fig. 11 & Fig. S25, S26).

In the ground state, electron density in HOMO of **L** distributed mainly on dihydroxy group substituted benzene ring along with the hydroxyl groups and binding atoms, whereas, LUMO of probe distributed over both the benzene ring along with coordinating sites. On the other side, electron crowd in HOMO of **L**-Zn^{2+} is mainly populated on the *tert*- butyl group substituted benzene ring along with coordinating sites whereas, the LUMO of **L**-Zn^{2+} was redistributed on dihydroxy group substituted benzene ring along with the hydroxyl groups and coordinating atoms.

The probe exhibits a peak at 302 (λ_{exp} 290) nm which is assigned to π-π^* and it is mainly associated with 75.03% orbital contribution from HOMO-3 to LUMO, a peak at 307 (λ_{exp} 299) nm which is assigned to n- π^* with an orbital contribution of 87.97% due to HOMO-1 to LUMO transition and a peak at 356 (λ_{exp} 340) nm which is due to charge transfer process with an orbital contribution of 98.22% due to HOMO to LUMO transition. The **L**-Zn^{2+} exhibits a peak at 321 (λ_{exp} 370) nm that is principally associated to 94.73% orbital contribution from HOMO-2 to LUMO, a peak at 349 (λ_{exp} 390) nm with an orbital contribution of 97.44% due to HOMO-1 to LUMO and a peak at 397 (λ_{exp} 429) nm which is largely associated to 98.69% orbital contribution from HOMO to LUMO (Fig. S14 and Table 3 & 4). The **L** exhibits a band gap of 4.08 eV while **L**-Zn^{2+} shows 3.47 eV (Fig. 11). These results are in good agreement with the experimentally observed results [58]. Furthermore, we have also compared the stabilities of **L** and **L**-Zn^{2+} complex by calculating chemical hardness ($\eta = \frac{E_{LUMO}-E_{HOMO}}{2}$). The chemical hardness value for **L** (2.04 eV) is high as compared to its Zinc complex (1.73 eV) indicating its higher stability [59–61].

3.6. pH dependent fluorescence studies

The effect of pH on the fluorescence behavior of **L** in the presence and absence of Zinc (II) ion was undertaken over a 3–11 pH in order to extend its biological application using PBS (Phosphate buffer saline) solution. The sensor is silent from pH 2–6 due to protonation of nitrogen atom whereas it dramatically increases from 7 to 11 due to deprotonation of hydroxyl groups. The Zinc complex exhibits weak fluorescence in the region 2–6 due to protonation of hydroxyl groups and suddenly increases from 8 to 11. A formation of stable complex in basic media switch on the CHEF process giving high fluorescence intensity (Fig. S15) [25,62].

3.7. Solvent effect

The fluorescence intensity of **L** in different solvents such as Ethanol, Acetone, Dimethylformamide, Chloroform, Methanol, Dichloromethane, Dimethyl sulfoxide, Ethyl acetate, Tetrahydrofuran and Hexane was examined in order to know the emissive efficiency of probe in different solvents. Electronic and fluorescence spectra of optical probe depends on the nature of solvent in which it is immersed. Some processes such as proton or charge exchange between solute and solvent, hydrogen bond formation, solvent dependent aggregation, isomerization equilibria ionization, and physical interactions between solute and solvent molecules have significant effect on the electronic spectrum of the probe [63]. An optical probe displays high fluorescence intensity in polar protic solvents due to inhibition of ESIPT process (Fig. S16) [64].

3.8. Reversible nature of probe

Developing an optical probe with reversibility is a very important parameter in sensing metal ions. Reversible nature of **L** for Zn^{2+} ion in 4% aqueous acetonitrile medium was investigated using well known metal ion chelator EDTA. Upon adding the EDTA solution to L-Zn^{2+} complex, it abstract the Zn^{2+} ion from complex and the sensor was regenerated at 481 nm. The fluorescence intensity at 485 nm quenches due to formation of EDTA-Zn^{2+} complex and

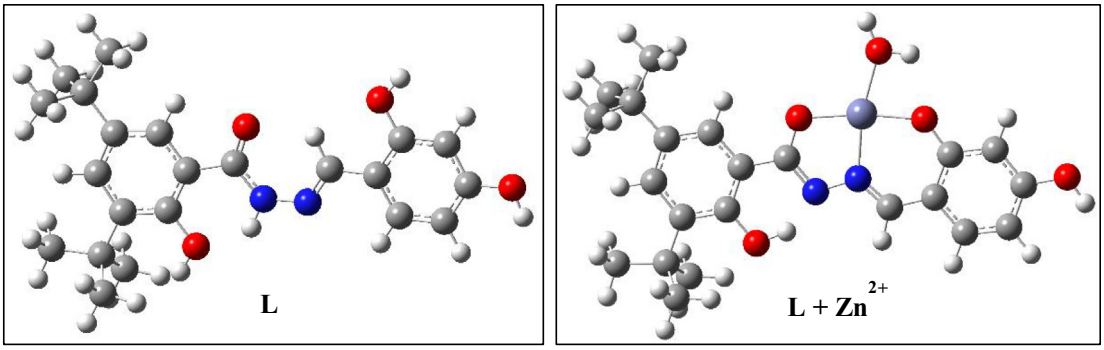

Fig. 10. The energy-minimized structures of (a) L and (b) L-Zn^{2+}.

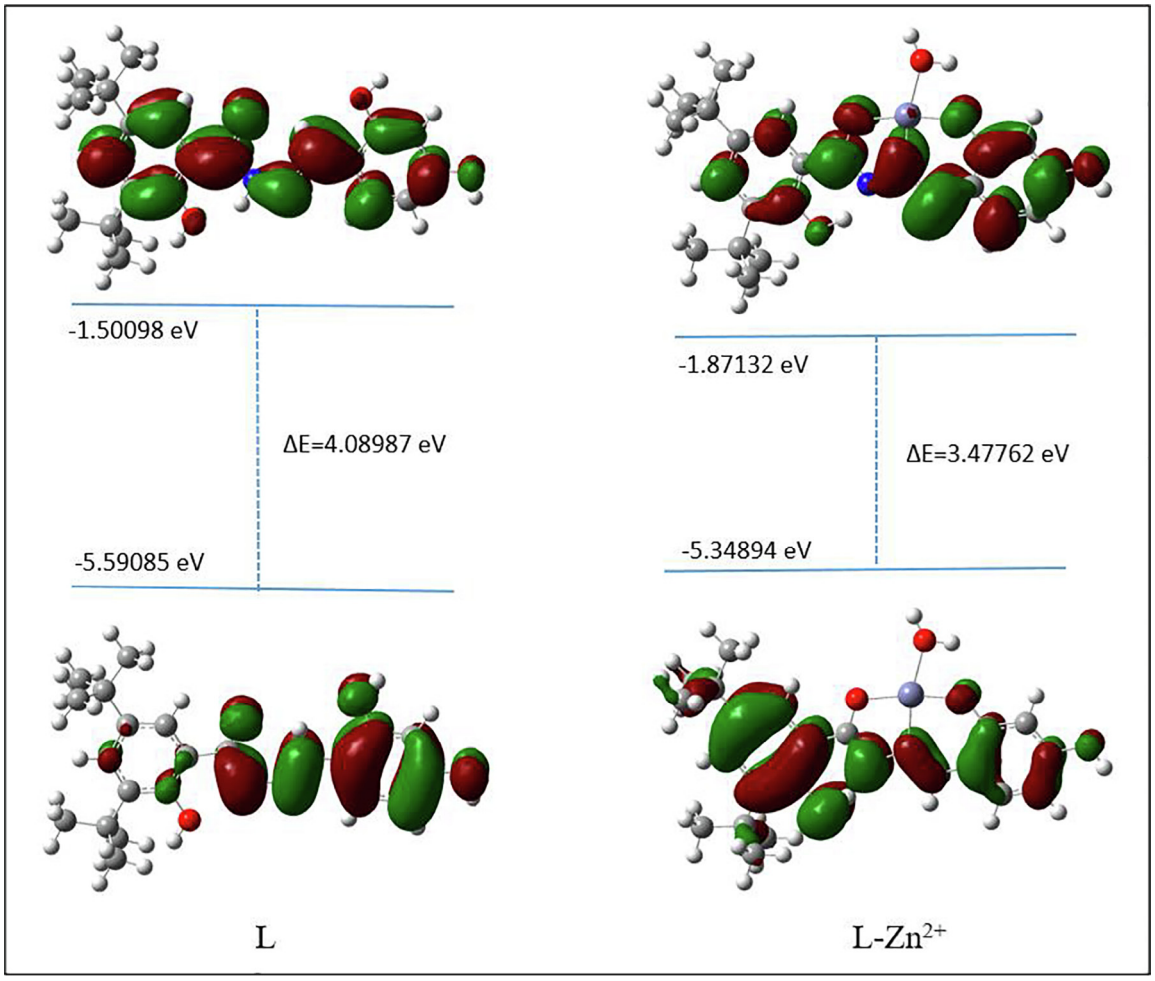

Fig. 11. A HOMO-LUMO energy band gap diagram of **L** and **L** -Zn^{2+}.

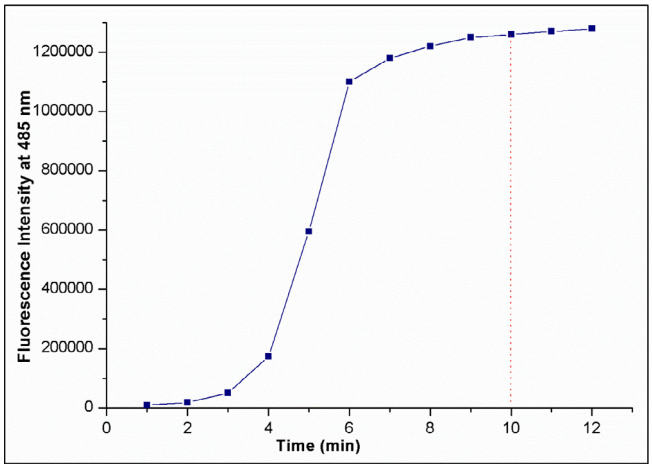

Fig. 12. A HOMO-LUMO energy band gap diagram of **L** and **L** -Zn^{2+}.

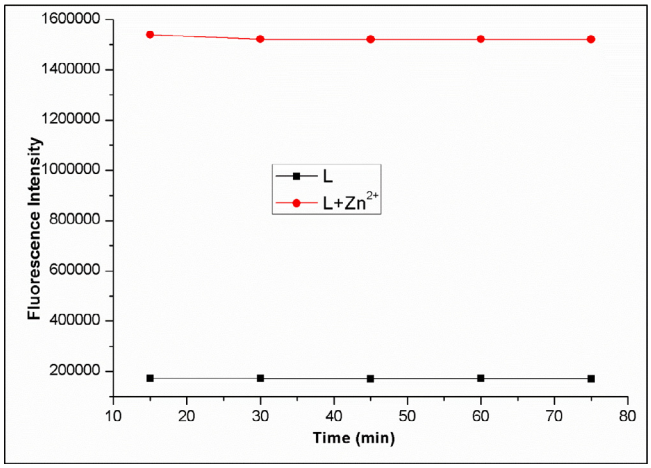

Fig. 13. Fluorescence enhancing profile of addition of Zn^{2+} to L from 0 to 12 min.

colored solution becomes colorless. Again, adding Zn^{2+} ions to EDTA-Zn^{2+} complex, sensor displays a fluorescence intensity at 485 nm and colorless solution becomes colored due to formation of **L**-Zn^{2+} and this process repeats over few cycles. Thus, the use of EDTA can lead to regeneration of **L** from the Zn^{2+}complex. Therefore, probe may be reused for further sensing of Zn^{2+} (Fig. S17) [65,66].

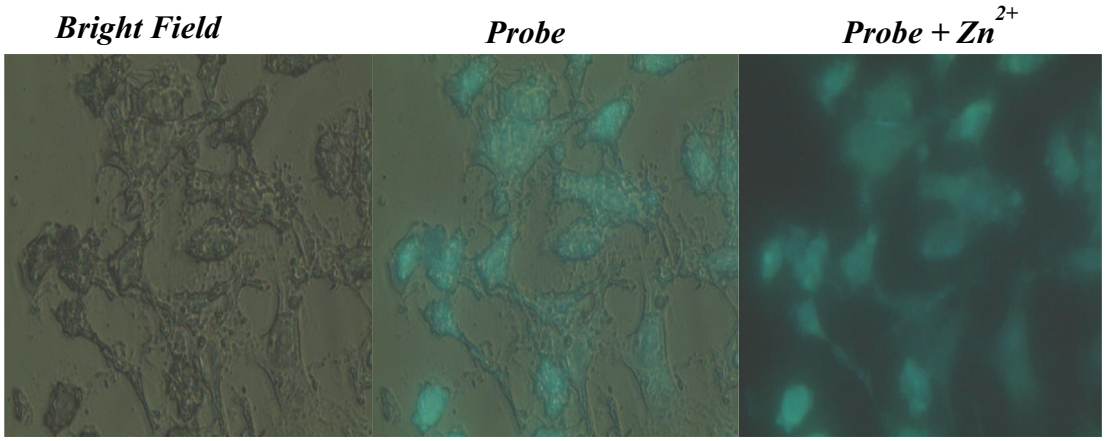

Fig. 14. Fluorescent imaging of HeLa cells incubated with L followed by the addition of Zn^{2+}. The cells were incubated with L (10 μM) for 30 min, washed with PBS, and incubated with 10 μM of Zn^{2+}. λ_{ex} = 340 nm, λ_{em} = 481 nm.

3.9. Response time and photostabilities

The time in which the **L** recognizes Zn^{2+} and forms Zinc complex is an important parameter for fast real time detection. To the 4% aqueous acetonitrile solution of **L**, 15 equivalent of Zn^{2+} was added and its fluorescence intensity at 485 nm was measured at every minute using fluorescence spectrophotometer. The fluorescence intensity of bare probe at 481 nm remains constant for an hour indicating its higher stability. Upon adding Zinc, its fluorescence intensity increases at 485 nm within 6 min indicating its high reactivity towards metal and remains constant afterwards indicating its high stability at 298 K (Figs. 12 & 13) [25].

3.10. Cytotoxicity and bio imaging

Practical applications of **L** for recognition of biologically important Zinc ion was explored through cell imaging experiment. Before cell imaging experiment, cytotoxicity of sensor and its Zinc complex was checked by performing MTT assay in HeLa cells. HeLa cells were incubated with various concentrations (12.5, 25, 50 100 and 200 μM) of **L** for 24 h and results indicate that HeLa cells treated with 12.5 μM of **L** showed no severe cytotoxicity with cell viability about 97.67% (Fig. S18).

To explore the sensing ability of **L** for Zinc, we have performed cell imaging experiment (Fig. 14). Initially, HeLa cells were treated with 10 μM solution of **L** for 4 h at 37 °C and fluorescence images were taken. Sensor was found to be cell permeable and displays weak fluorescence. Upon incubating preloaded HeLa cell with 10 μM Zn^{2+} ion, cells exhibit obvious strong green fluorescence. These results indicate that, sensor **L** is permeable into HeLa cells and binds to intracellular Zn^{2+} ion by exhibiting a high fluorescence [63].

4. Conclusions

In summary, we have synthesized novel fluorophore (**L**) and characterized by various spectroscopic techniques. Among different metal ions tested, probe selectively sense Zinc ion by giving turn on optical response. Based on the experimental and theoretical results we proposed a dual (ESIPT/ICT) mechanism responsible for selective sensing of Zinc ion. The binding constant estimated was well within the reported values for Zinc in literature (10^1-10^{12}). The detection limit of **L** for Zinc ion is at nanomolar level. We could regenerate **L** by adding an EDTA salt to the solution of L-Zn^{2+} complex. Probe shows high emission in polar protic solvents due to blockage of ESIPT process. The sensor recognizes the presence of Zinc in HeLa cells with high cell viability. Finally we believe that, the present sensor could certainly contribute in the field of developing new optical sensor by logical structural design.

CRediT authorship contribution statement

Mahantesh Budri: Conceptualization, Methodology, Validation, Formal analysis, Investigation, Writing - original draft, Visualization. **Ramesh Vadavi:** Validation, Investigation. **Prajakta Kadolkar:** Software, Formal analysis, Data curation. **Shivaraj Patil:** Software, Formal analysis, Data curation. **Kalagouda Gudasi:** Investigation, Resources, Supervision, Project administration. **Sanjeev Inamdar:** Investigation, Resources, Supervision.

Declaration of Competing Interest

The authors declare that they have no known competing financial interests or personal relationships that could have appeared to influence the work reported in this paper.

Acknowledgements

The authors thank USIC, Karnatak University, Dharwad for electronic spectral analyses and Indian Institute of Science, Bangalore for recording NMR spectra. One of the authors (Mahantesh. B. Budri) is grateful to UGC for awarding a RFSMS fellowship.

Appendix A. Supplementary data

Supplementary data to this article can be found online at https://doi.org/10.1016/j.poly.2021.115046.

References

[1] J.M. Lehn, Supramolecular Chemistry - Concepts and Perspectives, VCH, Weinheim, 1995.
[2] B. Valeur, Molecular Luminescence Spectroscopy-Methods and Applications, Part-3, John, Wiley & sons, New York, 1993, p. 25.
[3] A. Hazra, A. Roy, A. Mukherjee, G.P. Maiti, P. Roy, Dalton Trans. 47 (2018) 13972.
[4] N. Roy, S. Nath, A. Dutta, P. Mondal, P.C. Paul, T.S. Singh, RSC Adv. 6 (2016) 63837.
[5] J. Bhosale, U. Fegade, B. Bondhopadhyay, S. Kaur, N. Singh, A. Basu, R. Dabur, R. Bendre, A. Kuwar, J. Mol. Recognit. 28 (2015) 369.
[6] K. Chantalakana, N. Choengchan, P. Yingyuad, P. Thongyoo, Tetrahedron Lett. 57 (2016) 1146.
[7] N. Roy, A.R.H. Pramanik, P.C. Paul, T. Sanjoy Singh, Spectrochim. Acta A 140 (2015) 150.

[8] J. Zhu, Y. Zhang, Y. Chen, T. Sun, Y. Tang, Y. Huang, Q. Yang, D. Maa, Y. Wang, M. Wang, Tetrahedron Lett. 58 (2017) 365.
[9] T. Xu, H. Duan, X. Wang, X. Meng, J. Bu, Spectrochim. Acta A 138 (2015) 603.
[10] R.G. Pearson, Chemical Hardness: Applications from Molecules to Solids, Wiley-VCH, New York, 1997.
[11] S.S. Zumdahl, Chemical Principles, 5th Edition., Houghton Mifflin, Boston, 2005.
[12] X. Qian, Y. Xiao, Y. Xu, X. Guo, J. Qiana, W. Zhu, ChemCom 46 (2010) 6418.
[13] J. Wu, W. Liu, J. Ge, H. Zhang, P. Wang, Chem. Soc. Rev. 40 (2011) 3483.
[14] J. Li, C. Yin, F. Huo, Dyes Pigm. 131 (2016) 1156.
[15] K. Li, X. Wang, A. Tong, Anal. Chim. Acta 776 (2013) 69.
[16] S. Dey, A. Roy, G.P. Maiti, S.K. Mandal, P. Banerjee, P. Roy, New J. Chem. 40 (2016) 1365.
[17] S. Chowdhury, B. Rooj, A. Dutta, U. Mandal, J. Fluoresc. 28 (2018) 999.
[18] R.S. Kumar, S.K. Ashok Kumar, K. Vijayakrishna, A. Sivaramakrishna, P. Paira, C. V.S. Brahmmnanad Rao, N. Sivaraman, S.K. Sahoo, New J. Chem. 00 (2013) 1.
[19] W.N. Wu, P.D. Mao, Y. Wang, X.L. Zhao, Z.Q. Xu, Z.H. Xu, Y. Xue, Spectrochim. Acta A 188 (2018) 324.
[20] C.A.H. Aguilar, T. Pandiyan, N. Singh, N. Jayanthi, Spectrochim. Acta A 146 (2015) 142.
[21] A.J. Sanchez, B. Ortiz, V.O. Navarrete, N. Farfan, R. Santillana, Analyst 00 (2013) 1.
[22] C. Chen, G. Men, W. Bu, C. Liang, H. Sun, S. Jiang, Sensor. Actuat. B-Chem. 220 (2015) 463.
[23] W.K. Dong, S.F. Akogun, Y. Zhang, Y.X. Sun, X.Y. Dong, Sensor. Actuat. B-Chem. 238 (2017) 723.
[24] V.K. Gupta, A.K. singh, L.K. Kumawat, N. Mergu, Sensor. Actuat. B-Chem. 222 (2016) 468.
[25] M. Kumar, A. Kumar, M.K. Singh, S.K. Sahu, Sensor. Actuat. B-Chem. 241 (2017) 1218.
[26] Y. Li, Q. Niu, T. Wei, Li Tianduo, Anal. Chim. Acta 1049 (2019) 196.
[27] N. Roy, H.A. Pramanik, P.C. Paul, S.T. Singh, J. Fluoresc. 24 (4) (2014) 1099.
[28] S. Santhi, S. Amala, S.M. Basheer, J. Chem. Sci. 11 (2018) 130.
[29] F.U. Rahman, A. Ali, R. Guo, J. Tian, H. Wang, Z.T. Li, D.W. Zhang, Sensor. Actuat. B-Chem. 211 (2015) 544.
[30] M. Hosseini, A. Ghafarlo, M.R. Ganjali, F. Faridbod, P. Norouzi, M. Salavati, Sensor. Actuat. B-Chem. 198 (2014) 411.
[31] R. Alam, T. Mistri, R. Bhowmick, A. Katarkar, K. Chaudhuri, M. Ali, RSC Adv. 6 (2016) 1268.
[32] J.H. Hu, J.B. Li, J. Qi, Y. Sun, Sensor. Actuat. B-Chem. 208 (2015) 581.
[33] Q. Niu, T. Sun, T. Li, Z. Guo, H. Pang, Sensor. Actuat. B-Chem. 266 (2018) 730.
[34] M. Shyamal, P. Mazumdar, S. Maity, S. Samanta, G.P. Sahoo, A. Misra, ACS Sens. 1 (6) (2016) 739.
[35] X. Wen, Q. Wang, Z. Fan, J. Lumin. 194 (2018) 366.
[36] A.K. Saini, M. Srivastava, V. Sharma, V. Mishraa, S.M. Mobin, Dalton Trans. 45 (2016) 3927.
[37] L. Subha, C. Balakrishnana, S. Natarajan, M. Theetharappan, B. Subramanian, M. A. Neelakantan, Spectrochim. Acta A 153 (2016) 249.
[38] J. Nie, N. Li, Z. Ni, Y. Zhao, L. Zhang, Tetrahedron Lett. 58 (2017) 1980.
[39] D. Maity, A. Mukherjee, S.K. Mandal, P. Roya, J. Lumin. 210 (2019) 508.
[40] R. Diana, U. Caruso, S. Concilio, S. Piotto, A. Tuzi, B. Panunzi, Dyes Pigm. 155 (2018) 249.
[41] B. Panunzi, R. Diana, S. Concilio, L. Sessa, A. Tuzi, S. Piotto, U. Caruso, J. Lumin. 212 (2019) 200.
[42] M. Budri, P. Kadolkar, K. Gudasi, S. Inamdar, Jrnl. Mol. Liquids 283 (2019) 346.
[43] B.K. Datta, D. Thiyagarajan, A. Ramesh, G. Das, Dalton Trans. 00 (2013) 1.
[44] H. Liu, Y. Dong, B. Zhang, F. Liu, C. Tan, Y. Tan, Y. Jiang, Sensor Actuat B-Chem 234 (2016) 616.
[45] P.S. Hariharan, S.P. Anthony, Anal. Chim. Acta 848 (2014) 74.
[46] R. Singh, A. Gogoi, G. Das, RSC Adv. 6 (2016) 112246.
[47] B.K. Datta, D. Thiyagarajan, S. Samanta, A. Ramesh, G. Das, Org. Biomol. Chem. 12 (2014) 4975.
[48] A. Hens, A. Maity, K.K. Rajak, Inorgan. Chim. Acta 423 (2014) 408.
[49] D. Udhayakumari, S. Saravanamoorthy, M. Ashok, V. Sivan, Tetrahedron Lett. 52 (2011) 4631.
[50] G.Y. Li, Han K. Li, Adv. Rev. 8 (2018) 1.
[51] K. Boonkitpatarakula, A. Smata, K. Kongnukoola, S. Srisurichan, K. Chainok, M. Sukwattanasinitta, J. Lumin. 198 (2018) 59.
[52] S. Chall, S.S. Mati, S. Konar, D. Singharoy, S.C. Bhattacharya, Org. Biomol. Chem. 12 (2014) 6447.
[53] B.K. Datta, D. Thiyagarajan, A. Ramesh, G. Das, Dalton Trans. 00 (2012) 1.
[54] D. Sarkar, A.K. Pramanik, T.K. Mondal, RSC Adv. 4 (2014) 25341.
[55] N. Roy, A. Dutta, P. Mondal, P.C. Paul, T. Sanjoy Singh, J. Fluoresc. 27 (2017) 1307.
[56] J. Qin, T. Li, B. Wang, Z. Yang, L. Fan, Spectrochim. Acta A 133 (2014) 38.
[57] D. Udhayakumari, S. Saravanamoorthy, M. Ashok, Sivan Velmathi, Tetrahedron Lett. 52 (2011) 4631.
[58] (a) S. S. Bhat, V. K. Revankar, V. Kumbar, K. Bhat, V. A. Kawade, Acta Cryst., C74 (2018) 146; (b) R. S. Kumara, S. K. Ashok Kumara, K. Vijayakrishnaa, A. Sivaramakrishnaa, P. Pairaa, C.V.S. Brahmmnanada Rao, N. Sivaraman, S. K. Sahoo, New J. Chem., 00 (2013) 1. (c) S. Bothra, L.T. Babu, P. Paira, S. K. Ashok Kumar, R. Kumar, S. K. Sahoo, Anal. Bioanal. Chem., 410 (1) (2018) 201.
[59] V. Kumar, A. Kumar, U. Diwan, S. Ramesh, S.K. Srivastava, K.K. Upadhyay, Sensor. Actuat. B-Chem. 207 (2015) 650.
[60] J.H. Hu, Y. Sun, J. Qi, Q. Li, T.B. Wei, Spectrochim. Acta A 175 (2017) 125.
[61] C.R. Lohani, J. Kim, S. Chung, J. Yoon, K. Lee, Analyst 135 (2010) 2079.
[62] M.M. Li, F.Wu. Wang, X.Y. Wang, T.T. Zhang, Y. Xu, Y. Xiao, J.Y. Miao, B.X. Zhao, Anal. Chim. Acta 826 (2014) 77.
[63] C.A. Barboza, A.L. Sobolewski, Phys. Chem. Chem. Phys. 00 (2013) 1.
[64] L.G.T.A. Duarte, J.C. Germino, C.D.A. Braga, C.A. Barboza, T.D.Z. Atvars, F.D.S. Santos, F.S. Rodembusch, Photochem. Photobiol. Sci. 17 (2018) 231.
[65] T.S. Singh, P.C. Paul, A.R.H. Pramanik, Spectrochim. Acta A 121 (2014) 520.
[66] J.C. Qin, L. Fan, B.D. Wang, Z.Y. Yang, T.R. Lia, Anal. Methods 7 (2015) 716.